

Sub-barrier enhancement of fusion as compared to a microscopic method in $^{18}\text{O}+^{12}\text{C}$

T. K. Steinbach, J. Vadas, J. Schmidt, C. Haycraft, S. Hudan, and R. T. deSouza*
Department of Chemistry and Center for Exploration of Energy and Matter, Indiana University
2401 Milo B. Sampson Lane, Bloomington, Indiana 47408, USA

L. T. Baby, S. A. Kuvin, and I. Wiedenhöver
Department of Physics, Florida State University, Tallahassee, Florida 32306, USA

A. S. Umar and V. E. Oberacker
Department of Physics and Astronomy, Vanderbilt University, Nashville, Tennessee 37235, USA
 (Dated: July 24, 2014)

Background: Measurement of the energy dependence of the fusion cross-section at sub-barrier energies provides an important test for theoretical models of fusion.

Purpose: To extend the measurement of fusion cross-sections in the sub-barrier domain for the $^{18}\text{O}+^{12}\text{C}$ system. Use the new experimental data to confront microscopic calculations of fusion.

Method: Evaporation residues produced in fusion of ^{18}O ions with ^{12}C target nuclei were detected with good geometric efficiency and identified by measuring their energy and time-of-flight. Theoretical calculations with a density constrained time dependent Hartree-Fock (DC-TDHF) theory include for the first time the effect of pairing on the fusion cross-section.

Results: Comparison of the measured fusion excitation function with the predictions of the DC-TDHF calculations reveal that the experimental data exhibits a smaller decrease in cross-section with decreasing energy than is theoretically predicted.

Conclusion: The larger cross-sections observed at the lowest energies measured indicate a larger tunneling probability for the fusion process. This larger probability can be associated with a smaller, narrower fusion barrier than presently included in the theoretical calculations.

PACS numbers: 21.60.Jz, 26.60.Gj, 25.60.Pj, 25.70.Jj

Understanding the origin of the elements, namely where and how they are formed, is one of the grand challenges in science [1]. Independent of where they are formed whether in stellar interiors [2, 3] or on earth [4–6], nucleosynthesis involves nuclear fusion. An accurate description of fusion is thus key to understanding nucleosynthesis. In recent years, fusion reactions have also been proposed to be important in exotic astrophysical environments, for example triggering X-ray superbursts that originate in the crust of an accreting neutron star [7]. The putative reactions involve fusion of neutron-rich light nuclei at sub-barrier energies [8–10]. Initial measurements of fusion induced with neutron-rich light nuclei suggest an enhancement of the fusion probability as compared to standard models of fusion-evaporation [11]. At sub-barrier energies one is particularly sensitive to the microscopic degrees-of-freedom as the two nuclei collide, hence a microscopic treatment is the most relevant. For reactions at sub-barrier energies, the initial interpenetration of the matter distributions of the two nuclei is small but at the inner turning-point the nuclei have significant overlap. Consequently, a theoretical approach that can accurately describe the matter distributions at the outer and inner turning-points is desirable. The time-dependent Hartree-Fock (TDHF) theory provides a prac-

tical foundation for a fully microscopic theory of large amplitude collective motion and is thus well suited to study low-energy fusion reactions [12, 13]. Recent advances provide a more realistic treatment of tunneling through the use of microscopically obtained heavy-ion potentials [14, 15]. To test the accuracy of these microscopic calculations, high quality experimental data is needed. In the present work, we present a measurement of the total fusion cross-section for $^{18}\text{O} + ^{12}\text{C}$ that extends one order of magnitude lower in cross-section than previous measurements. We utilize this data to compare to the microscopic calculations of fusion.

To conduct the experiment, a beam of ^{18}O ions with an intensity of $1.5\text{--}4\times 10^5$ p/s was accelerated to energies between $E_{\text{lab}} = 16.25$ MeV and $E_{\text{lab}} = 36$ MeV using the FN tandem at Florida State University's John D. Fox accelerator center. The beam was pulsed at a frequency of 12.125 MHz. As the beam energy is critical to the accurate measurement of the fusion excitation function, the accuracy of the accelerator energy calibration was checked using known proton resonance energies and determined to be within 7 keV. After passing through a microchannel plate (MCP) detector approximately 1 m upstream of the target (US MCP), the beam was incident on a $93\text{ }\mu\text{g}/\text{cm}^2$ thick ^{12}C foil which served as the target (TGT MCP) as depicted in Fig. 1a. The ^{12}C target foil also served as a secondary emission foil for a microchannel plate detector [16] thus providing a timing signal for a

* desouza@indiana.edu

time-of-flight (TOF) measurement. Measurement of the TOF between the two MCPs allows one to reject beam particles scattered or degraded prior to the target.

Earlier measurements of sub-barrier fusion for similar systems identified fusion events by measuring the γ -rays emitted by the fusion residues as they de-excited [17, 18]. While this approach, of tagging fusion through γ -rays, allows the use of thick targets and high intensity beams, it suffers from the low efficiency inherent in γ -ray detection and any uncertainties in the knowledge of the relevant decay channels. We have therefore elected to directly measure the fusion residues in order to determine the fusion cross-section.

Reaction products were detected in the angular range $4.3^\circ \leq \theta_{\text{lab}} \leq 11.0^\circ$ using a segmented, annular silicon detector which provided both an energy and fast timing signal [19]. Due to the kinematics of the reaction, the angular range subtended by this detector resulted in a high geometric efficiency for detection of fusion residues. Reaction products were distinguished on the basis of their energy and time-of-flight (ETO) [16]. A typical ETO spectrum measured is depicted in Fig. 1b where the energy corresponds to the energy deposited in the silicon detector while the time-of-flight is the time difference between the target MCP and the silicon detector.

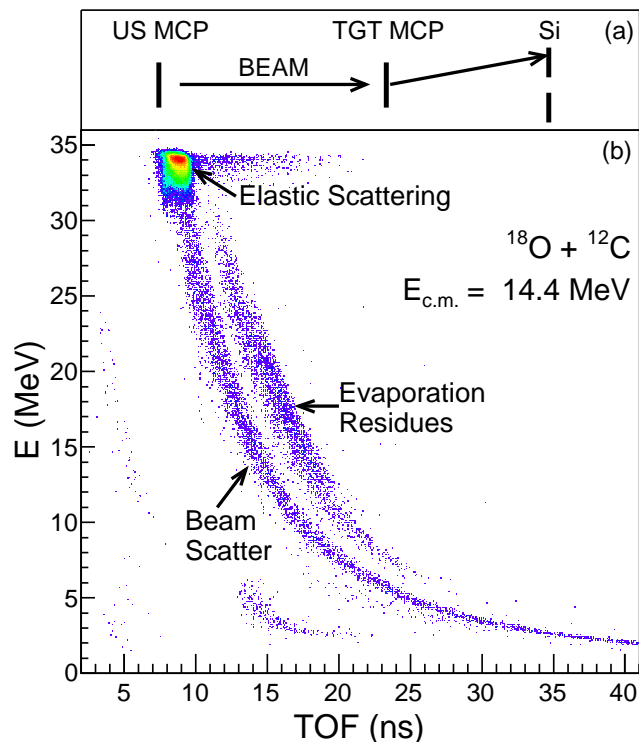


FIG. 1. (Color online) Top panel: Schematic illustration of the experimental setup. Bottom panel: Energy versus time-of-flight spectrum for ^{18}O ions incident on ^{12}C target nuclei at $E_{\text{c.m.}} = 14.4$ MeV. Color is used to represent yield in the two dimensional spectrum on a logarithmic scale.

The most prominent feature in Fig. 1b is the peak at E

≈ 34 MeV that corresponds to elastically scattered particles. Originating from this peak is a locus of points with lower energies and longer TOF values. Points in this locus are scattered beam particles. Visible at larger TOF and clearly separated from the beam scatter line is an island of reaction products. This island is populated by evaporation residues that result from fusion of the projectile and target nuclei to form a compound nucleus which subsequently de-excites. Protons and alpha particles which are emitted during this de-excitation cascade of the compound nucleus manifest themselves in the spectrum with a characteristic energy time-of-flight relationship. Alpha particles are observed with energies between 10 MeV and 25 MeV and TOF values of approximately 5 ns. Protons are observed at deposited energies of $E < 6$ MeV, consistent with the Si detector thickness, and TOF values of approximately 15 ns. The larger TOF values observed for protons as compared to the alpha particles is due to the slower risetime exhibited by protons and the leading edge discrimination employed. Also visible in the spectrum is a tail on the elastic peak which is constant in energy and extends to larger TOF values. This tail occurs with low probability (0.4%) as compared to the elastic peak.

The measured evaporation residue cross-section was ascertained by using the measured number of beam particles incident on the target, the measured number of evaporation residues, and the known target thickness. The total number of beam particles incident on the target was determined by counting the coincidences between the MCP at the target position and the upstream MCP. The number of residues detected was established by selecting the appropriate region of the ETO spectrum and summing the number of evaporation residues contained within it. The limits of the region of integration were established by calculating the TOF for different mass residues and using the beam scatter line as a reference. After accounting for the finite time resolution, an interval in mass number, $22 \leq A \leq 30$ was used for measurements at $E_{\text{c.m.}} > 7.5$ MeV and $24 \leq A \leq 30$ for $E_{\text{c.m.}} \leq 7.5$ MeV.

In order to determine the total fusion cross-section it is necessary to know the geometric efficiency of the experimental setup. The efficiency was determined by using a statistical model, *evapOR* [20], which simulates the decay of a compound nucleus using a Hauser-Feshbach approach. By calculating the fraction of the evaporation residues that lie within the detector acceptance, the geometric efficiency of the experimental setup is obtained. The bombarding energy dependent efficiency lies between 50% and 59%. Using the efficiency together with the measured evaporation residue cross-section, the total fusion cross-section is extracted. Since the MCP efficiency affects both the counting of the total number of beam particles and the number of evaporation residues, it does not impact the measured total fusion cross-section.

The measured excitation function is displayed in Fig. 2 along with previously published results [21–23]. As expected, the fusion cross-sections decrease with decreas-

ing $E_{c.m.}$ indicative of a barrier controlled phenomenon. It is noteworthy that even for the lowest energies measured an exponential decrease of the cross-section with decreasing energy is observed. Vertical error bars on the present data include both the statistical uncertainties as well as a 2% systematic error. This systematic error is

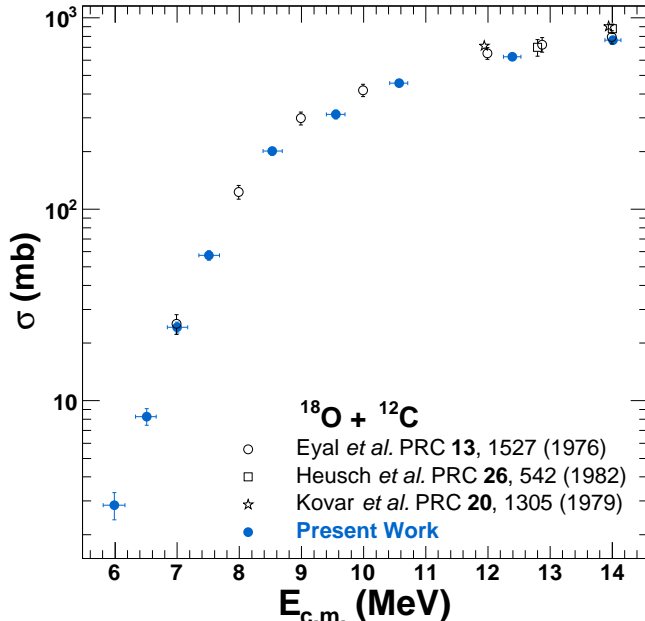


FIG. 2. (Color online) The fusion excitation function for $^{18}\text{O} + ^{12}\text{C}$ is shown at energies near and below the Coulomb barrier. Literature values are shown as open circles [21], open squares [23], and open stars [22] with the present data represented by solid circles.

associated with the analysis. Horizontal error bars represent the uncertainty in whether the fusion occurs at the front or back of the target foil. Using the direct measurement of evaporation residues as done in the present experiment, previous measurements only measured the fusion cross-section down to the 25 mb level [21]. In contrast, in the present work we measure the fusion cross-section down to the 2.8 mb level, close to a full order of magnitude lower in cross-section. At energies where the present dataset overlaps with existing data, overall agreement of the cross-sections is good, close to the statistical uncertainties of the prior measurements. This overall agreement not only indicates that our approach in extracting the fusion cross-section is sound but that there are no significant uncertainties in the values of the target thickness or detector efficiency. Closer comparison of the present dataset with the data of Ref. [21] indicates that the presently measured cross-sections are approximately 7% lower for $E_{c.m.} \geq 10$ MeV. While the prior measurements required integration of an angular distribution measured with a low geometric efficiency detector, the present measurement directly measures a large fraction of the evaporation residue yield. We therefore believe that the present cross-sections are more accurate. It

should be noted that the statistical quality of the present dataset is substantially better than that of the earlier measurements.

In recent years it has become possible to perform TDHF calculations on a 3D Cartesian grid thus not requiring any artificial symmetry restrictions and with much more accurate numerical methods [24–26]. In addition, the quality of the effective interactions has been substantially improved [27–31]. Over the past several years, the density constrained TDHF (DC-TDHF) method for calculating heavy-ion potentials [14] has been employed to calculate heavy-ion fusion cross-sections with remarkable success [5, 32]. While most applications have been for systems involving heavy nuclei, recently the theory was used to study above and below barrier fusion cross-sections for lighter systems, specifically for reactions involving various isotopes of O+O and O+C [33, 34] relevant for the reactions that occur in the neutron star crust. One general characteristic of TDHF and DC-TDHF calculations for light systems is that the fusion cross-section at energies well above the barrier are usually overestimated [35, 36], whereas an excellent agreement is found for sub-barrier cross-sections [33]. This is believed to be due to various breakup channels in higher energy reactions of these lighter systems that are not properly accounted for in TDHF dynamics and contribute to fusion instead. Nevertheless, the agreement is remarkable given the fact that the only input in DC-TDHF is the Skyrme effective N-N interaction, and there are no adjustable parameters.

An unfortunate consequence of the TDHF approach, however, is the inability to treat pairing during the collision process. This shortcoming in the inclusion of pairing has led to the prediction of deformation of the ground state for some even-even nuclei such as $^{18,20}\text{O}$ in disagreement with self-consistent mean field calculations that include pairing. To overcome this shortcoming, in prior work an average of all orientations of the deformed nucleus with respect to the target nucleus has been performed [34]. It can be qualitatively argued that this averaging nonetheless results in a larger fusion cross-section as compared to the spherical nucleus.

In this work we report for the first time on the inclusion of pairing in the DC-TDHF calculations. This was achieved by performing a BCS pairing calculation for the static solution of ^{18}O resulting in a spherical nucleus with a subsequent density constraint calculation to produce this density as a solution of the ordinary Hartree-Fock equations in the spirit of the density-functional theory. This nucleus with frozen occupations was then used in the TDHF time evolution. Subsequent density-constraint calculations in DC-TDHF method preserves this spherical shape during the entrance channel dynamics. As can be seen in Fig. 3a, inclusion of pairing in the DC-TDHF calculation for $^{18}\text{O} + ^{12}\text{C}$ results in a significant reduction of the fusion cross-section. The standard DC-TDHF calculations are presented as the dashed curve while the calculations that include pairing are depicted

as the solid curve. At all energies, pairing acts to reduce the fusion cross-section. At the highest energies shown pairing reduces the cross-section to $\approx 80\%$ of the value calculated without pairing. This difference between the calculations with and without pairing increases dramatically as the incident energy decreases. At the lowest energies shown the introduction of pairing in the calculation reduces the cross-section to $\approx 36\%$ of the cross-section calculated without pairing.

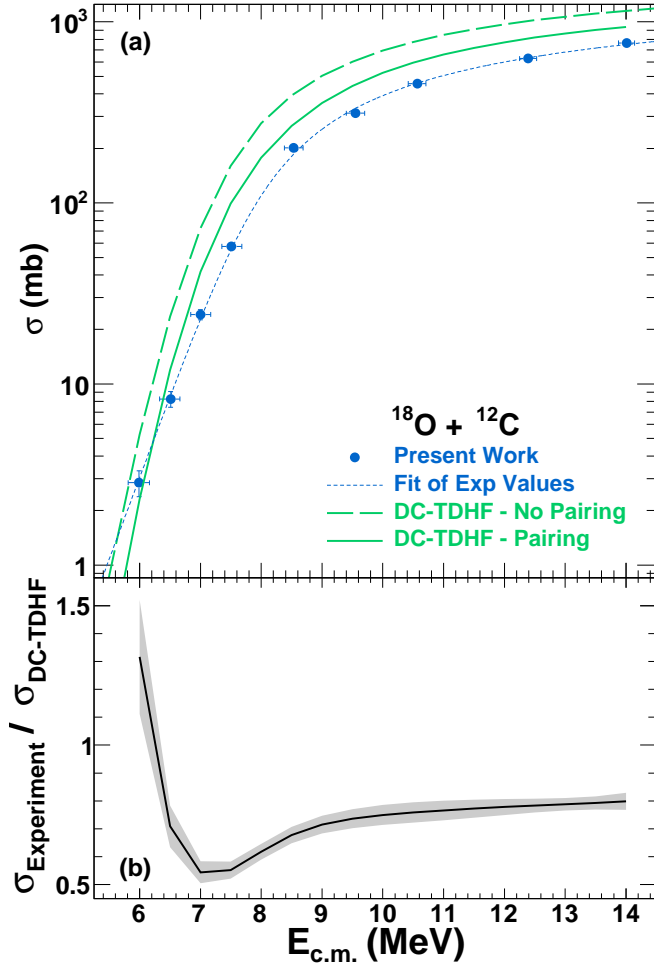


FIG. 3. (Color online) Top panel: Comparison of the experimentally measured fusion cross-sections (closed symbols) with the results of the DC-TDHF calculations with (solid line) and without (dashed line) pairing. Also shown, as a dotted line, is the result of a fit to the experimental data (see text for details). Bottom panel: Energy dependence of the ratio of the experimentally measured cross-sections to the DC-TDHF predictions which include pairing. The shaded band depicts the uncertainty in the ratio due to the uncertainty in the experimental cross-sections.

Comparison of the experimental fusion excitation function with the DC-TDHF microscopic calculations is presented in Fig. 3a. The presently measured fusion cross-sections, previously shown in Fig. 2, are indicated as solid symbols. Overall comparison of the experimental

cross-sections with the DC-TDHF calculations indicate that the experimental cross-sections are lower than the theoretical predictions. In order to facilitate a quantitative comparison of the experimental excitation function with the theoretical predictions, we have fit the experimental cross-sections with a functional form [37] that describes the penetration of an inverted parabolic barrier:

$$\sigma = \frac{R_c^2}{2E} \hbar\omega \cdot \ln \left\{ 1 + \exp \left[\frac{2\pi}{\hbar\omega} (E - V) \right] \right\} \quad (1)$$

where R_c is the radius of the fusion barrier, V is the height of the interaction barrier, ω is the frequency, and E is the incident energy. The best fit achieved using this functional form is shown as the dotted line in Fig. 3a and has values of $R_c = 7.24 \pm 0.16$ fm, $V = 7.62 \pm 0.14$ MeV, and $\hbar\omega = 2.78 \pm 0.29$ MeV, remarkably the calculated DC-TDHF barrier also has a barrier height of 7.60 MeV. Shown in Fig. 3b is the ratio of the fit of the experimentally measured cross-sections to the DC-TDHF calculations with pairing. For energies $E_{c.m.} > 9$ MeV, the ratio $\sigma_{\text{Experiment}}/\sigma_{\text{DC-TDHF}}$ is ≈ 0.75 and decreases weakly with decreasing energy. A stronger decrease in the ratio is observed as the energy decreases from $E_{c.m.} = 9$ MeV to $E_{c.m.} = 7$ MeV. At this energy, the ratio is minimum with a value of 0.54. As the incident energy decreases further, the ratio increases reaching a value of 1.32 at the lowest energy measured, $E_{c.m.} = 6$ MeV. The presence of breakup reactions at energies above the barrier could explain the fact that the ratio is less than unity in this energy range. With decreasing incident energy, the role of breakup reactions diminishes hence the ability of the DC-TDHF method to describe fusion is expected to improve. We therefore focus our attention on the comparison of the model and experiment in the sub-barrier region. The key feature in the ratio is therefore its change with decreasing incident energy in the sub-barrier domain, specifically its increase from a value smaller than unity to a value larger than unity. This trend emphasizes that the experimental and theoretical excitation functions have different shapes with the experimental cross-section falling more slowly with decreasing incident energy than is theoretically predicted by the DC-TDHF method. This enhancement of the experimental fusion cross-sections relative to the DC-TDHF predictions is a factor of ≈ 2.4 as the incident energy decreases from $E_{c.m.} = 7$ MeV to $E_{c.m.} = 6$ MeV. We have assessed the impact of the experimental uncertainties on the ratio presented and display the result as a shaded band in Fig. 3b. It is clearly evident that the trends exhibited by the ratio are significantly larger than the magnitude of the uncertainties.

The fact that the sub-barrier experimental fusion cross-sections decrease more slowly with decreasing energy than the calculated cross-sections can be interpreted as a larger tunneling probability for the experimental data as compared to the theoretical calculations. This enhanced tunneling probability can be associated with a narrower barrier, which deviates from an inverted

parabolic shape. The fundamental reason that the barrier determined from the experimental data is weaker than in the theory is presently unclear. It should also be recalled that within the DC-TDHF calculations, inclusion of pairing decreased the predicted cross-sections. It was assumed that the initial occupation numbers calculated with pairing were frozen as the reaction dynamics proceeded. It can be argued that relaxing this stringent condition would result in larger cross-sections. Unfortunately, microscopic calculations which allow the pairing to evolve in response to changes in the shape of the nuclear system as the fusion proceeds are beyond the scope of the present work. Such calculations would provide a more realistic treatment of the impact of pairing on fusion. It is noteworthy that the previous experimental data [21] only extended down to $E_{c.m.} = 7$ MeV. The dramatic increase in cross-section relative to the DC-TDHF

method occurs at energies below $E_{c.m.} = 7$ MeV. This enhancement of the fusion cross-section in the sub-barrier domain demonstrates the importance of measuring the sub-barrier fusion cross-section for light, heavy-ion reactions. This sub-barrier cross-section enhancement could yield new insight into the fusion dynamics of neutron-rich light nuclei.

We wish to acknowledge the support of the staff at Florida State University's John D. Fox accelerator in providing the high quality beam that made this experiment possible. This work was supported by the U.S. Department of Energy under Grant No. DE-FG02-88ER-40404 (Indiana University) and Grant No. DE-FG02-96ER40975 (Vanderbilt University) and the National Science Foundation under Grant No. PHY-1064819 (Florida State University).

-
- [1] *2007 NSAC Long Range Plan: The Frontiers of Nuclear Science* (2007).
 - [2] Y. Penionzhkevich, *Physics of Atomic Nuclei* **73**, 1460 (2010).
 - [3] P. F. F. Carnelli *et al.*, *Phys. Rev. Lett.* **112**, 192701 (2014).
 - [4] V. I. Zagrebaev, A. V. Karpov, and W. Greiner, *Phys. Rev. C* **85**, 014608 (2012).
 - [5] B. B. Back, H. Esbensen, C. L. Jiang, and K. E. Rehm, *Rev. Mod. Phys.* **86**, 317 (2014).
 - [6] R. Yanez *et al.*, *Phys. Rev. Lett.* **112**, 152702 (2014).
 - [7] T. Strohmayer and L. Bildsten, *Compact X-ray Stellar Sources* (Cambridge University, 2006) p. 113.
 - [8] C. J. Horowitz, H. Dussan, and D. K. Berry, *Phys. Rev. C* **77**, 045807 (2008).
 - [9] C. J. Horowitz, O. L. Caballero, and D. K. Berry, *Phys. Rev. E* **79**, 026103 (2009).
 - [10] C. J. Horowitz and D. K. Berry, *Phys. Rev. C* **79**, 065803 (2009).
 - [11] M. J. Rudolph *et al.*, *Phys. Rev. C* **85**, 024605 (2012).
 - [12] J. W. Negele, *Rev. Mod. Phys.* **54**, 913 (1982).
 - [13] C. Simenel, *Eur. Phys. J. A* **48**, 152 (2012).
 - [14] A. S. Umar and V. E. Oberacker, *Phys. Rev. C* **74**, 021601(R) (2006).
 - [15] K. Washiyama and D. Lacroix, *Phys. Rev. C* **78**, 024610 (2008).
 - [16] T. K. Steinbach *et al.*, *Nucl. Instr. and Meth.* **A743**, 5 (2014).
 - [17] B. Cujec and C. A. Barnes, *Nucl. Phys. A* **266**, 461 (1976).
 - [18] P. R. Christensen, Z. E. Switkowski, and R. A. Dayras, *Nucl. Phys. A* **280**, 189 (1977).
 - [19] R. T. deSouza *et al.*, *Nucl. Instr. and Meth.* **A632**, 133 (2011).
 - [20] N. G. Nicolis and J. R. Beene, unpublished (1993).
 - [21] Y. Eyal, M. Beckerman, R. Chechik, Z. Fraenkel, and H. Stocker, *Phys. Rev. C* **13**, 1527 (1976).
 - [22] D. G. Kovar, D. F. Geesaman, T. H. Braid, Y. Eisen, W. Henning, T. R. Ophel, M. Paul, K. E. Rehm, S. J. Sanders, P. Sperr, J. P. Schiffer, S. L. Tabor, S. Vigdor, B. Zeidman, and F. W. Prosser, Jr., *Phys. Rev. C* **20**, 1305 (1979).
 - [23] B. Heusch, C. Beck, J. P. Coffin, P. Engelstein, R. M. Freeman, G. Guillaume, F. Haas, and P. Wagner, *Phys. Rev. C* **26**, 542 (1982).
 - [24] A. S. Umar, M. R. Strayer, J. S. Wu, D. J. Dean, and M. C. Güçlü, *Phys. Rev. C* **44**, 2512 (1991).
 - [25] A. S. Umar and V. E. Oberacker, *Phys. Rev. C* **73**, 054607 (2006).
 - [26] J. A. Maruhn, P.-G. Reinhard, P. D. Stevenson, and A. S. Umar, *Comp. Phys. Comm.* **185**, 2195 (2014).
 - [27] P.-G. Reinhard, A. S. Umar, K. T. R. Davies, M. R. Strayer, and S.-J. Lee, *Phys. Rev. C* **37**, 1026 (1988).
 - [28] A. S. Umar, M. R. Strayer, P.-G. Reinhard, K. T. R. Davies, and S.-J. Lee, *Phys. Rev. C* **40**, 706 (1989).
 - [29] E. Chabanat, P. Bonche, P. Haensel, J. Meyer, and R. Schaeffer, *Nucl. Phys. A* **635**, 231 (1998).
 - [30] P. Klüpfel, P.-G. Reinhard, T. J. Bürvenich, and J. A. Maruhn, *Phys. Rev. C* **79**, 034310 (2009).
 - [31] M. Kortelainen, T. Lesinski, J. Moré, W. Nazarewicz, J. Sarich, N. Schunck, M. V. Stoitsov, and S. Wild, *Phys. Rev. C* **82**, 024313 (2010).
 - [32] R. Kesper, A. S. Umar, and V. E. Oberacker, *Phys. Rev. C* **85**, 044606 (2012).
 - [33] A. S. Umar, V. E. Oberacker, and C. J. Horowitz, *Phys. Rev. C* **85**, 055801 (2012).
 - [34] R. T. deSouza, S. Hudan, V. E. Oberacker, and A. S. Umar, *Phys. Rev. C* **88**, 014602 (2013).
 - [35] C. Simenel, R. Kesper, A. S. Umar, and V. E. Oberacker, *Phys. Rev. C* **88**, 024617 (2013).
 - [36] A. S. Umar, C. Simenel, and V. E. Oberacker, *Phys. Rev. C* **89**, 034611 (2014).
 - [37] C. Y. Wong, *Phys. Rev. Lett.* **31**, 766 (1973).